gdu

Human 'brite/beige' adipocytes develop from capillary networks, and their implantation improves metabolic homeostasis in mice

So Yun Min^{1,2}, Jamie Kady^{1,3}, Minwoo Nam^{2,4}, Raziel Rojas-Rodriguez^{1,2}, Aaron Berkenwald⁵, Jong Hun Kim¹, Hye-Lim Noh¹, Jason K Kim¹, Marcus P Cooper⁴, Timothy Fitzgibbons⁴, Michael A Brehm^{1,3} & Silvia Corvera¹

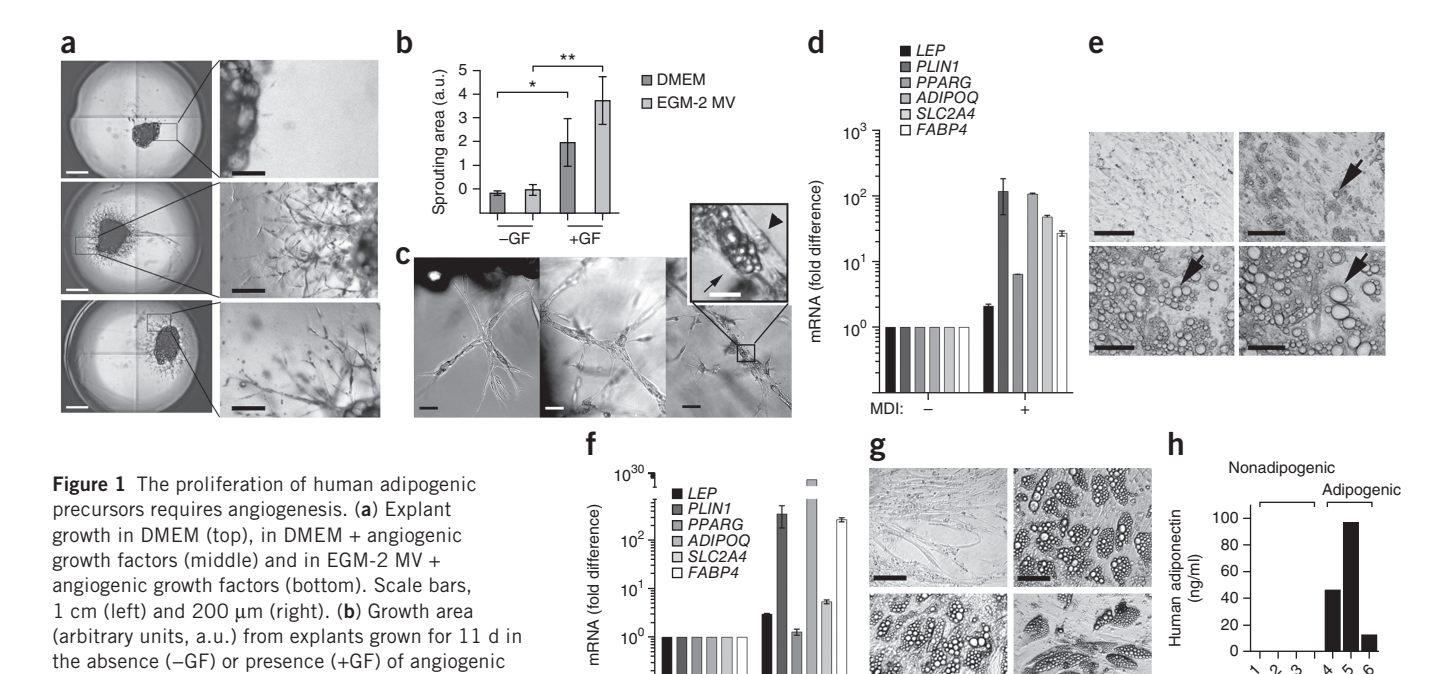
Uncoupling protein 1 (UCP1) is highly expressed in brown adipose tissue, where it generates heat by uncoupling electron transport from ATP production. UCP1 is also found outside classical brown adipose tissue depots 1-4, in adipocytes that are termed 'brite' (brown-in-white) or 'beige'. In humans, the presence of brite or beige (brite/beige) adipocytes is correlated with a lean, metabolically healthy phenotype⁵⁻⁸, but whether a causal relationship exists is not clear. Here we report that human brite/beige adipocyte progenitors proliferate in response to pro-angiogenic factors, in association with expanding capillary networks. Adipocytes formed from these progenitors transform in response to adenylate cyclase activation from being UCP1 negative to being UCP1 positive, which is a defining feature of the beige/brite phenotype, while displaying uncoupled respiration. When implanted into normal chow-fed, or into high-fat diet (HFD)-fed, glucoseintolerant NOD-scid IL2rgnull (NSG) mice, brite/beige adipocytes activated in vitro enhance systemic glucose tolerance. These adipocytes express neuroendocrine and secreted factors, including the pro-protein convertase PCSK1, which is strongly associated with human obesity. Pro-angiogenic conditions therefore drive the proliferation of human beige/brite adipocyte progenitors, and activated beige/brite adipocytes can affect systemic glucose homeostasis, potentially through a neuroendocrine mechanism.

During human embryonic development, adipocytes first emerge from nascent vascular networks⁹, and lineage-tracing studies have demonstrated that adipocyte progenitors reside in the walls of adult mouse adipose tissue capillaries^{10–13}. These findings suggest that the proliferation of adipocyte and vascular progenitors may be interdependent. To determine whether human adipocyte progenitors proliferate in conjunction with adipose tissue capillaries, we used an *in vitro* system in which microvessels develop from adipose tissue fragments.

Explants from human subcutaneous adipose tissue from individuals undergoing panniculectomy surgery (Supplementary Table 1) were embedded in Matrigel and cultured in Dulbecco's modified Eagle's medium (DMEM) + 10% fetal bovine serum (FBS), or in endothelial cell growth medium-microvascular (EGM2-MV) either in the absence or in the presence of the pro-angiogenic growth factors vascular endothelial growth factor (VEGF), human fibroblast growth factor B (hFGF-B), human epidermal growth factor (hEGF), or long R3 insulin-like growth factor 1 (R3-IGF-1) (Fig. 1a), and they were then imaged after 10 d in culture. Capillary growth was negligible in explants cultured in either DMEM of EGM-2 MV in the absence of growth factors, but it was clearly measurable in DMEM or EGM-2 MV in the presence of these factors (Fig. 1b). Maximal growth was seen in EGM2-MV, which is consistent with the optimized pro-angiogenic properties of this medium. Over time, cells at the tips of the sprouts projected thin filopodia into the gel, and then divided and aligned to form thicker branches (Fig. 1c), which previously have been seen to include endothelial and nonendothelial cells^{14,15}. To determine whether any of these cells correspond to adipocyte progenitors, we exposed cultures to adipogenic conditions. Because the activation of peroxisome proliferator-activated receptor gamma (PPARγ) by ligands such as thiazolidenediones can induce lipid accumulation in cells independently of adipogenic conversion¹⁶, we used a minimal adipogenic cocktail of 3-isobutyl-1-methylxanthine, dexamethasone and insulin (MDI). After ~6 d, we observed a loss of continuity between the cells that form the capillary structure and the lipid droplets that are in cells within the capillaries (Fig. 1c). These morphological changes were accompanied by the induction of classical adipocyte markers (Fig. 1d). These results were reproduced in explants from all panniculectomy samples that we studied (Supplementary Table 1), although the magnitude of the induction of individual markers varied. Thus, proliferation of human adipocyte progenitors occurs in conjunction with capillary growth and is critically dependent on pro-angiogenic growth factors.

¹Program in Molecular Medicine, University of Massachusetts Medical School, Worcester, Massachusetts, USA. ²Graduate School of Biomedical Sciences, University of Massachusetts Medical School, Worcester, Massachusetts Medical School, Worcester, Massachusetts, USA. ³Diabetes Center of Excellence, University of Massachusetts Medical School, Worcester, Massachusetts, USA. ⁴Cardiovascular Center of Excellence, University of Massachusetts Medical School, Worcester, Massachusetts, USA. ⁵Clinical Translational Research Pathway, University of Massachusetts Medical School, Worcester, Massachusetts, USA. Correspondence should be addressed to S.C. (silvia.corvera@umassmed.edu).

Received 24 September 2015; accepted 14 December 2015; published online 25 January 2016; doi:10.1038/nm.4031



individuals (n=12). Statistical significance was calculated using the Mann-Whitney test. *P < 0.05, **P < 0.01. (c) High-resolution representative images of explants (n=27 images per time point) grown for 5 (left), 12 (middle) or 18 (right) d; explants were exposed to MDI at day 12. Arrowhead indicates elongated cells forming the sprouts, and arrow indicates lipid droplets. Scale bars, 200 μ m and 50 μ m (inset). (d) qPCR for adipocyte-specific genes indicated in nondifferentiated (-MDI) or differentiated (+MDI) explants 7 d after the induction of differentiation qPCR results are expressed as the fold over the minimum detectable value for each gene among the experimental groups being compared. Plotted are the means, and error bars represent the range of two technical replicates from a representative experiment that has been replicated a minimum of three times with cells from separate individuals. Where error bars are not apparent, replicates were too close to result in a visible error bar. (e) A representative field (n=30 images from independent wells) of capillary network cells at days 0 (top left), 6 (top right), 12 (bottom left) and 18 (bottom right) after the induction of differentiation; arrows indicate the growth of lipid droplets inside a single adipocyte. Scale bars, 50 μ m. (f) qPCR for genes indicated in nondifferentiated (-MDI) or differentiated (+MDI) cells 7 d after the induction of differentiation. Plotted are the means and range of two technical replicates, of a representative experiment that has been replicated a minimum of three times with cells from separate individuals. (g) Example images (n=1, although 35 independent clones were examined in total) of three adipogenic, and one nonadipogenic, clones, which were identified by lipid droplet content. Scale bars, 50 μ m. (h) Human adiponectin concentration, detected in culture medium from three nonadipogenic, and three adipogenic, clones.

To determine whether the proliferation and/or differentiation of adipocyte progenitors required intercellular interactions within the capillary or interactions with Matrigel components, we generated singlecell suspensions from the microvessels, passaged them once on standard tissue culture dishes and subjected them to differentiation. We found that numerous cells differentiated into adipocytes, which were identifiable by lipid droplets that increased in size and coalesced over time (Fig. 1e), and by the induction of adipocyte genes (Fig. 1f). We obtained similar results in capillary-network cells from all explants studied, although the magnitude of the induction of individual genes varied. To determine whether single adipocyte progenitors are capable of autonomous growth and differentiation, we sorted live single cells individually into wells of 384-well plates. As is expected from cells of nonhematopoietic lineage, these cells were CD45⁻ (Supplementary Fig. 1). Cells that formed colonies (~10% of seeded cells) could be further passaged into 96-well plates; of these cells, ~75% underwent adipogenic differentiation, as determined morphologically by assessing lipid droplet accumulation (Fig. 1g) and functionally by measuring the secretion of adiponectin into the culture medium (Fig. 1h). Thus, human adipocyte progenitors isolated from capillary networks can be clonally expanded, and they can undergo differentiation in a cell-autonomous manner.

growth factors. Plotted data are means and s.e.m. taken from six explants per condition from two different

To determine whether cells generated from capillary networks include brite/beige adipocytes, we stimulated cultures acutely and

chronically with the adenylate cyclase activator forskolin (Fsk), and we analyzed thermogenic gene expression by means of real-time PCR (qPCR) (Fig. 2a). UCP1 mRNA was almost undetectable before and after adipogenic differentiation, but it was induced rapidly in response to the presence of Fsk, and it remained elevated with chronic exposure to the drug, as were mRNA levels of the canonical brown fat-cell genes cell death-inducing DFFA (DNA fragmentation factor-α)like effector A (CIDEA) and deiodinase 2 (DIO2) (Fig. 2a). We also detected genes in human cells that had been previously identified in mouse adipocyte progenitors, including integrin beta 1 (CD29), CD24, platelet-derived growth factor receptor alpha (PDGFRA) and zinc-finger protein 423 (ZNF423), as well as genes that are known to be enriched in brite/beige adipocytes and in human and mouse adipose tissue¹⁷ (**Supplementary Fig. 2**). To determine whether cells responded to the physiological stimuli that cause 'browning' in vivo, we compared the responses of nondifferentiated and differentiated cells to the presence of Fsk and isoproterenol (Fig. 2b). No induction was seen in nondifferentiated cells, but differentiated adipocytes responded to both stimuli (Fig. 2b). Notably, the human-selective β3-adrenergic agonist Mirabegron, which activates thermogenesis in human supraclavicular fat18, was more potent than the murineselective β3 agonist CL316,243 in inducing UCP1 expression in differentiated cells (Fig. 2b), which is consistent with the presence of functional β3-adrenergic receptors in these human adipocytes.

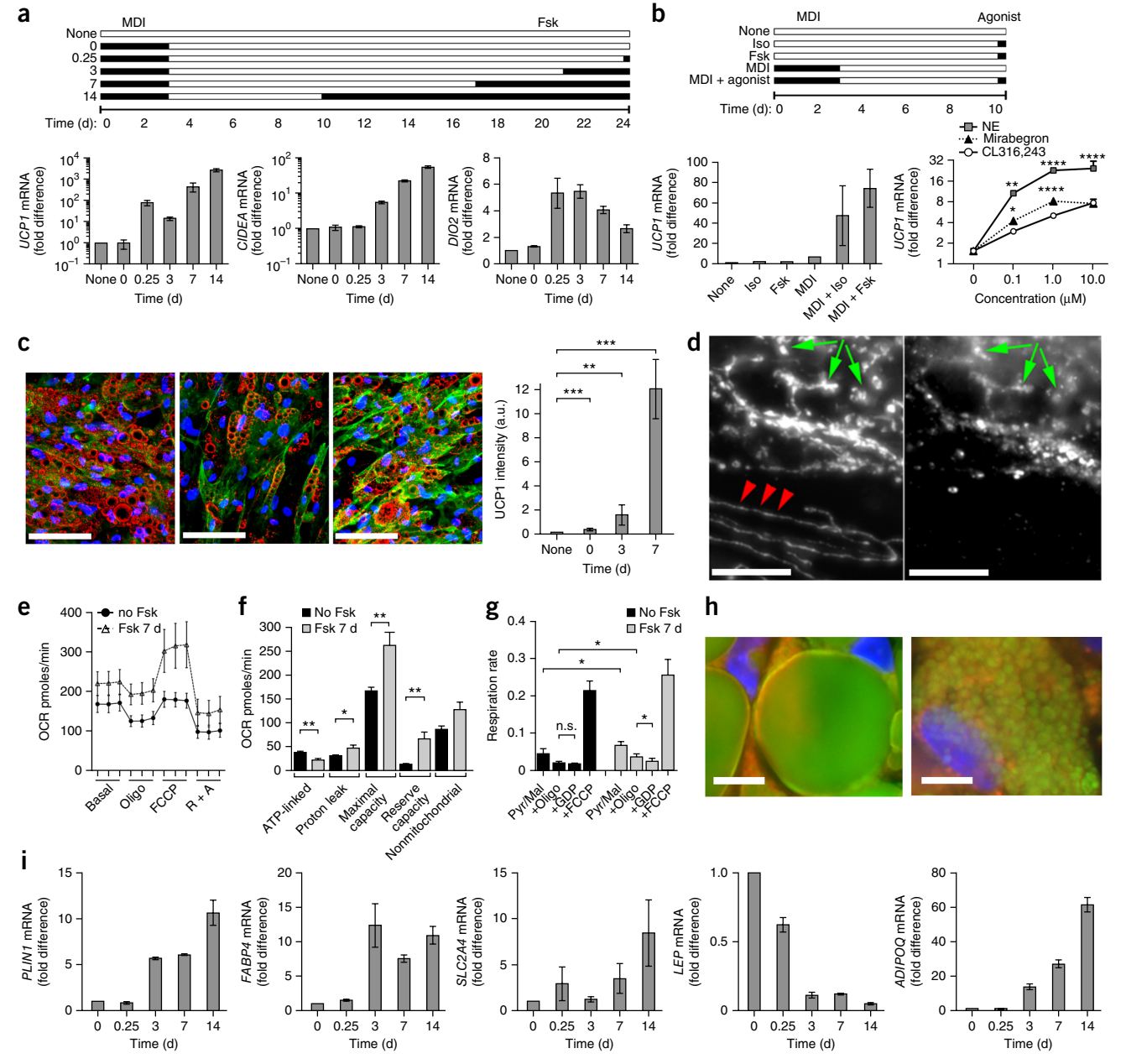


Figure 2 The induction of a human brite/beige phenotype in adipocytes derived from capillary networks. (a) Experimental scheme (top) and qPCR of indicated genes (bottom). Results are expressed as the fold over the minimum detectable value for each gene among the experimental groups being compared. Plotted are the means, and error bars represent the range of two technical replicates from a representative experiment that has been replicated a minimum of three times with cells from separate individuals. Where error bars are not apparent, replicates were too close to result in a visible error bar. (b) Experimental scheme (top) and UCP1 mRNA expression (bottom left) in cells exposed to isoproterenol (Iso) or forskolin (Fsk), as indicated in the scheme, or in response to different concentrations of adrenergic agonists (bottom right). Plotted are means \pm s.e.m. of three biological replicates (n = 3). The statistical difference relative to CL316,243 was determined at each concentration using Student's t test, corrected for multiple comparisons using the Holm-Sidak method. *P < 0.05, **P < 0.01, ****P < 0.0001. (c) Representative images (n = 30 images (ten fields each of cells from three separate individuals)) of differentiated cells exposed to Fsk for 0 (left), 3 (middle) and 7 (right) d, showing UCP1 (green), lipid droplets (red) and nuclei (blue). Scale bars, 200 µm. Plotted are means ± s.e.m. of UCP1 staining intensity from two fields per coverslip, of cells from three different individuals (n = 6). Statistical significance was assessed using the Mann-Whitney test versus nondifferentiated cells. **P < 0.01, ***P < 0.001. (d) Mitochondrial heat-shock protein 70 (Hsp70; left) and UCP1 (right) in adipocytes exposed to Fsk for 1 week. Arrowheads indicate linear mitochondrial structures in cells devoid of UCP1. Arrows indicate rounded mitochondrial structures that contain both UCP1 and Hsp70. Scale bars, 20 µm. (e) Oxygen consumption rate (OCR) of adipocytes exposed to vehicle (dimethyl sulfoxide 0.005%) or Fsk for 1 week. Plotted are the means ± s.e.m. of four experiments assayed in triplicate (n = 4). (f) Summary data for oxygen consumption parameters, calculated as described in Online Methods, derived from the means ± s.e.m. of cells from four separate individuals assayed in triplicate (n = 4). Statistical significance was assessed using two-tailed unpaired Student's t test. *P < 0.05, **P < 0.005. (g) OCR by digitoninpermeabilized adipocytes exposed to vehicle or Fsk for 1 week. Plotted are the means \pm s.e.m. of four experiments (n = 4). Statistical significance assessed using two-tailed unpaired Student's t test. *P < 0.05. n.s., not significant. (h) Lipid droplets (green), mitochondria (red) and nuclei (blue) in adipocytes without (left) or with (right) exposure to Fsk for 14 d. Scale bars, 20 μm. (i) qPCR of indicated genes, expressed as the fold relative to t = 0. Shown are mean values and ranges for two technical replicates. These results have been replicated a minimum of three times with cells from separate individuals.

The Fsk-induced increase in *UCP1* mRNA levels translated into an increase in protein, given that UCP1 was detected by immunofluorescence in most adipocytes, and that fluorescence intensity progressively increased upon chronic exposure to Fsk (**Fig. 2c**). Mitochondria containing UCP1 were rounded, dense and abundant (**Fig. 2d**), a feature reminiscent of brown adipose tissue mitochondria¹⁹. In contrast, interspersed cells with no detectable UCP1 contained the linear, sparse mitochondria (**Fig. 2d**).

The UCP1 expressed in these human adipocytes was functional, as cells treated chronically with Fsk displayed enhanced basal and uncoupled oxygen consumption compared to nontreated cells (Fig. 2e). In addition, mitochondrial parameters after the addition of specific inhibitors (Fig. 2f) revealed decreased ATP-linked oxygen consumption and enhanced proton leak in Fsk-treated cells compared to nontreated cells. The enhanced proton leak was at least in part attributable to the presence of UCP1, given that respiratory rate was inhibited in response to 1 mM guanosine diphosphate (GDP) in digitonin-permeabilized cells (Fig. 2g). We also observed other changes consistent with known properties of thermogenic adipocytes, including the remodeling of large lipid droplets into numerous small lipid droplets (Fig. 2h)^{20,21}, accompanied by a large increase in the expression of PLIN1 (perilipin 1) over time (Fig. 2i), which is consistent with an increase in droplet surface area. We observed increased expression of FABP4 (fatty acid binding protein 4) and SLC2A4 (also known as GLUT4, encoding solute carrier family 2 (facilitated glucose transporter), member 4, which are involved in the uptake of lipids and glucose, as well as decreased expression of LEP (leptin) and increased expression of ADIPOQ (adiponectin) in Fsk-treated cells compared to nontreated cells (Fig. 2i). This pattern is consistent with circulating concentrations of these adipokines in mice treated with 'probrowning' β3-adrenergic agonists²². Thus, adipocytes derived from human capillary networks possess the cardinal biochemical and physiological characteristics of brite/beige cells.

To determine the similarity of brite/beige adipocytes generated from human capillary networks to cells in human thermogenic fat, we obtained pericarotid adipose tissue from four individuals undergoing elective carotid endarterectomy (Supplementary Table 1). Relative to the expression of ADIPOQ, we found substantial variability in the expression of UCP1 and DIO2 among samples of pericarotid fat (Fig. 3a), but where values were higher, they were comparable to those seen in brite/beige adipocytes from capillary networks. Thus, these adipocytes resemble thermogenic adipose tissue in humans. We next asked whether human brite/beige cells could be functional in vivo. Cells were grown, differentiated and stimulated with Fsk as described in Online Methods. We routinely obtained cultures with unilocular and multilocular adipocytes, collected them by trypsinization, resuspended them in Matrigel and implanted them into the dorsal region of NSG mice (Fig. 3b). 11 weeks after implantation, we observed only solidified remains of the gel in the dorsal region under the skin of mice receiving only Matrigel (Fig. 3b). In contrast, we observed welldelineated vascularized adipose tissue structures in mice implanted with cell suspensions (Fig. 3b). These structures were clearly demarcated from surrounding tissue, and they contained large patches of adipocytes and vasculature (Fig. 3c). Human adipocytes were viable and integrated into the mouse circulation; we detected human adiponectin in serum from mice harboring implanted cells, but not in serum from mice receiving Matrigel only (Fig. 3d). Remarkably, implanted adipocytes maintained the brite/beige phenotype: we detected human-specific UCP1 and PLIN1 expression in the adipose tissue structure at levels comparable to those found in cells before

implantation (Fig. 3e), and we observed multilocular adipocytes in the excised structure (Supplementary Fig. 3).

We next asked whether human brite/beige cells could affect glucose metabolism. Mice implanted with cells displayed lower fasting glucose (Fig. 3f) and a more-rapid glucose disposal rate (Fig. 3g) than did those receiving Matrigel only. NSG mice have been reported to be highly resistant to HFD-induced obesity²³. Because susceptibility to HFD-induced obesity and glucose intolerance are enhanced by thermoneutrality²⁴, we subjected a cohort of NSG mice to a HFD at 30 °C. Within 2 weeks, mice displayed significant glucose intolerance (Fig. 3h). At 2 weeks of HFD feeding, mice were randomized to receive either Matrigel alone or brite/beige adipocytes suspended in Matrigel, as described above. Seven weeks after implantation, glucose tolerance was higher (Fig. 3i) and liver steatosis was lower (Fig. 3j) in mice that received cells than in those that received only Matrigel. Thus, brite/beige adipocytes derived from human capillary networks can enhance glucose metabolism in mice both under normal conditions and in the context of impaired glucose tolerance.

Although this is, to our knowledge, the first description of transplanted human adipocytes improving systemic glucose homeostasis, it has been reported that mouse subcutaneous adipose tissue can improve glucose homeostasis in HFD-fed mice²⁵. To determine whether the improvement in glucose tolerance seen in mice implanted with capillary-derived human adipocytes was indeed attributable to the cells' brite/beige characteristics, we compared the effects of nonactivated adipocytes to those of Fsk-activated adipocytes. We used hyperinsulinemic-euglycemic clamps *in vivo* to measure whole-body glucose turnover, which was normalized to circulating human adiponectin to adequately control for the quantity and the functional integration of implanted human cells. Mice implanted with Fskactivated cells displayed faster glucose turnover than did those implanted with nonstimulated cells (Fig. 4a), which demonstrated that the brite/beige phenotype directly contributed to the improvement of glucose metabolism. Indeed, this value is likely to be underestimated, as adiponectin expression is higher in Fsk-activated than in nonactivated brite/beige adipocytes (Fig. 2i). We noted a strong correlation between serum human adiponectin and whole-body glucose turnover when we analyzed the entire cohort of mice with nonactivated and Fsk-activated cells (Fig. 4b), which suggests that nonactivated cells were also capable of affecting glucose turnover, or that the cells became activated after transplantation. qPCR analysis of the implanted structures revealed detectable UCP1 expression in tissue formed from nonactivated cells, albeit at lower levels than those seen in tissue formed from Fsk-activated cells (Fig. 4c). These results support the conclusion that cells derived from human capillary networks give rise to brite/beige adipocytes, which can be activated in vitro and in vivo, and that these cells can positively affect glucose homeostasis.

To determine whether the enhanced glucose tolerance seen in mice implanted with brite/beige adipocytes was related to the thermogenic properties of these cells, body temperature was measured using subcutaneously implanted Thermochron iButton temperature loggers, which have a resolution of 0.025 °C and were set to record at 30-min intervals. Mice bred at room temperature harboring brite/beige adipocytes did not differ markedly from Matrigel controls in their basal body temperatures, or in their responses to cold exposure (Fig. 4d). It remains possible that local thermogenic effects, which are undetectable using whole-body temperature measurements, contribute to improved glucose metabolism. Alternatively, implanted cells might contribute to glucose tolerance independently of thermogenesis.



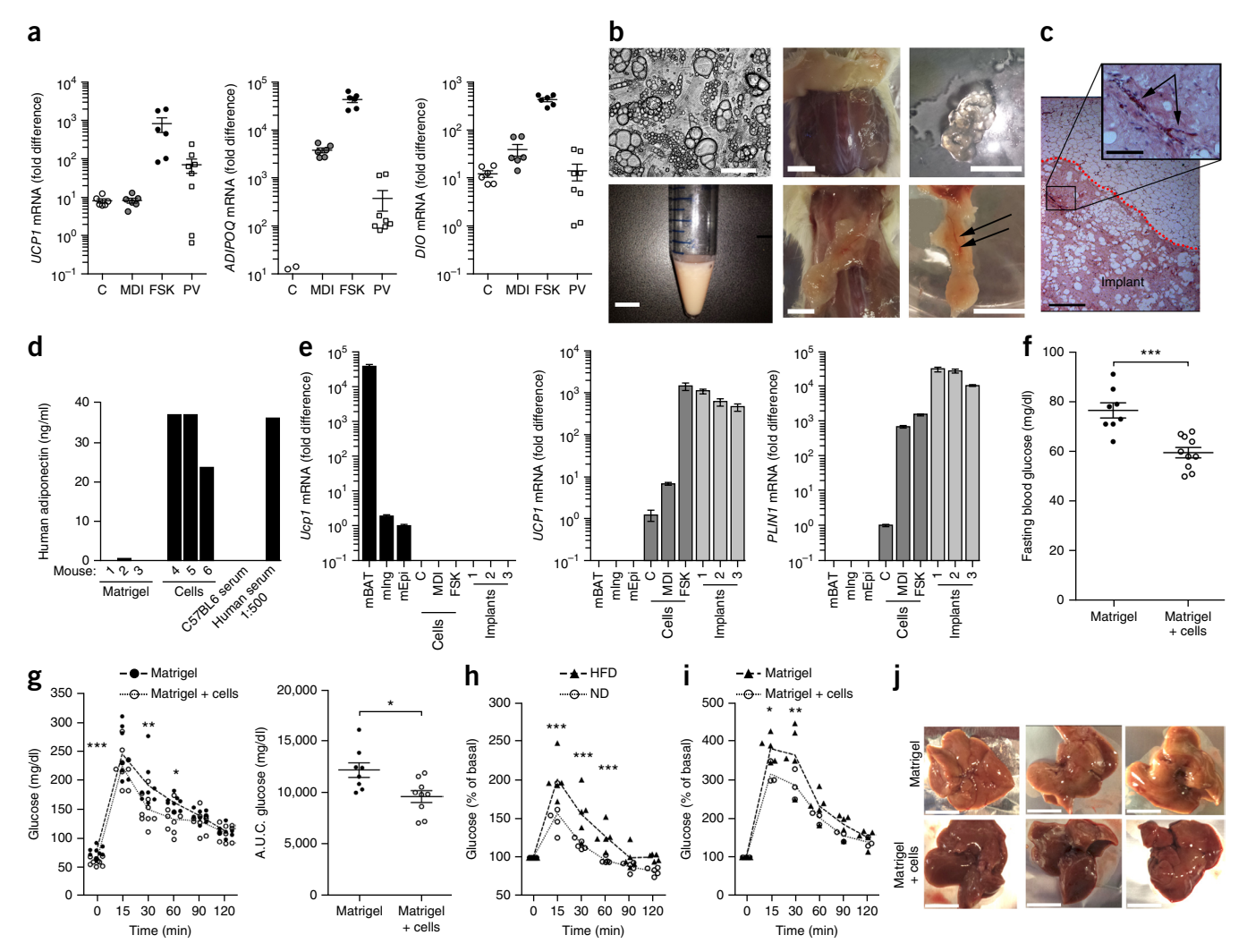


Figure 3 Characteristics and metabolic effects of human brite/beige adipocytes derived from capillary networks. (a) qPCR for indicated genes in nondifferentiated (C), differentiated (MDI) and Fsk-treated adipocytes (FSK), and in perivascular adipose tissue (PV). Values represent fold difference over the lowest detectable value in the series for the respective probe set. Plotted are means \pm s.e.m. for two technical replicates of samples from three (cells) or four (PV) individuals. (b) Phase image of cells for implantation (top left); suspension of cells (bottom left); dorsal area of mouse injected with Matrigel alone (top middle); collected remnants of the hydrogel (top right); dorsal area of mouse injected with cells (bottom middle); excised adipose structure (bottom right, scale bar) displaying vascularization (arrows). Scale bars, 100 µm (top left) and 1 cm. (c) Representative H&E staining of implants (n = 40 sections with five sections from each of eight independent implants); dotted red line separating the implant from surrounding mouse adipose tissue; blood vessels within the implant (arrow). Scale bars, 300 μm and 75 μm (inset). Similar results were seen in eight additional implants. (d) Human adiponectin in sera from six mice implanted with either Matrigel alone or cells in Matrigel, in serum from a control C57BL6 mouse and in a 1:500 dilution of normal human serum. (e) qPCR for mouse Ucp1, human UCP1 and human PLIN1 in mouse adipose depots (mBAT (mouse brown adipose tissue), mIng (mouse inguinal adipose tissue) and mEpi (mouse epididymal adipose tissue), human capillary-derived cells (C, MDI and FSK), and adipose structures from three mice, excised 7 weeks after implantation. Values represent the fold difference relative to the lowest detectable value in the series for each respective probe set; a value of 0 was given to nondetectable values. Error bars represent the range of two technical replicates. (f,g) Fasting glucose levels (f), glucose tolerance curves (g; left) and areas under the curve (A.U.C.) of the glucose excursion after a 16-h fast in male mice implanted with Matrigel (n = 8) or with Matrigel + cells (n = 10). (h) Glucose tolerance curves after an 8-h fast in mice housed at 30 °C for 2 weeks and fed either a normal diet (n = 5) or a 60% HFD (n = 5). (i) Glucose-tolerance curves after 11 weeks of 60% HFD feeding and an 8 h fast in mice housed at 30 °C, implanted with either Matrigel (n = 5) or Matrigel + cells (n = 3) after 2 weeks of a HFD. Statistical analysis was performed using two-tailed unpaired Student's t test at each time point of glucose-tolerance curves, and a Mann-Whitney test between groups for fasting blood glucose and area under the curves. *P < 0.05, **P < 0.01, ***P < 0.001 for f-i. (j) Livers from mice used in i immediately after euthanasia at 11 weeks. Scale bars, 1 cm.

To determine whether glucose uptake into implanted cells contributes to glucose turnover, we measured $2-[^{14}C]$ -deoxyglucose uptake into tissues during hyperinsulinemic-euglycemic clamps. On a per gram of tissue basis, the rate of glucose uptake by implanted cell structures was significantly higher than that of epididymal white fat, but lower than that of interscapular brown fat in the same animal (**Fig. 4e**). Because

the density of cells in the implant is lower than that in tissue because of dilution with Matrigel, these values may underestimate glucose consumption by human cells. Thus, improved glucose tolerance may be in part attributable to glucose consumption by implanted cells. However, whole-body glucose turnover was not directly correlated with the amount of glucose uptake by the implanted cells (Fig. 4f),



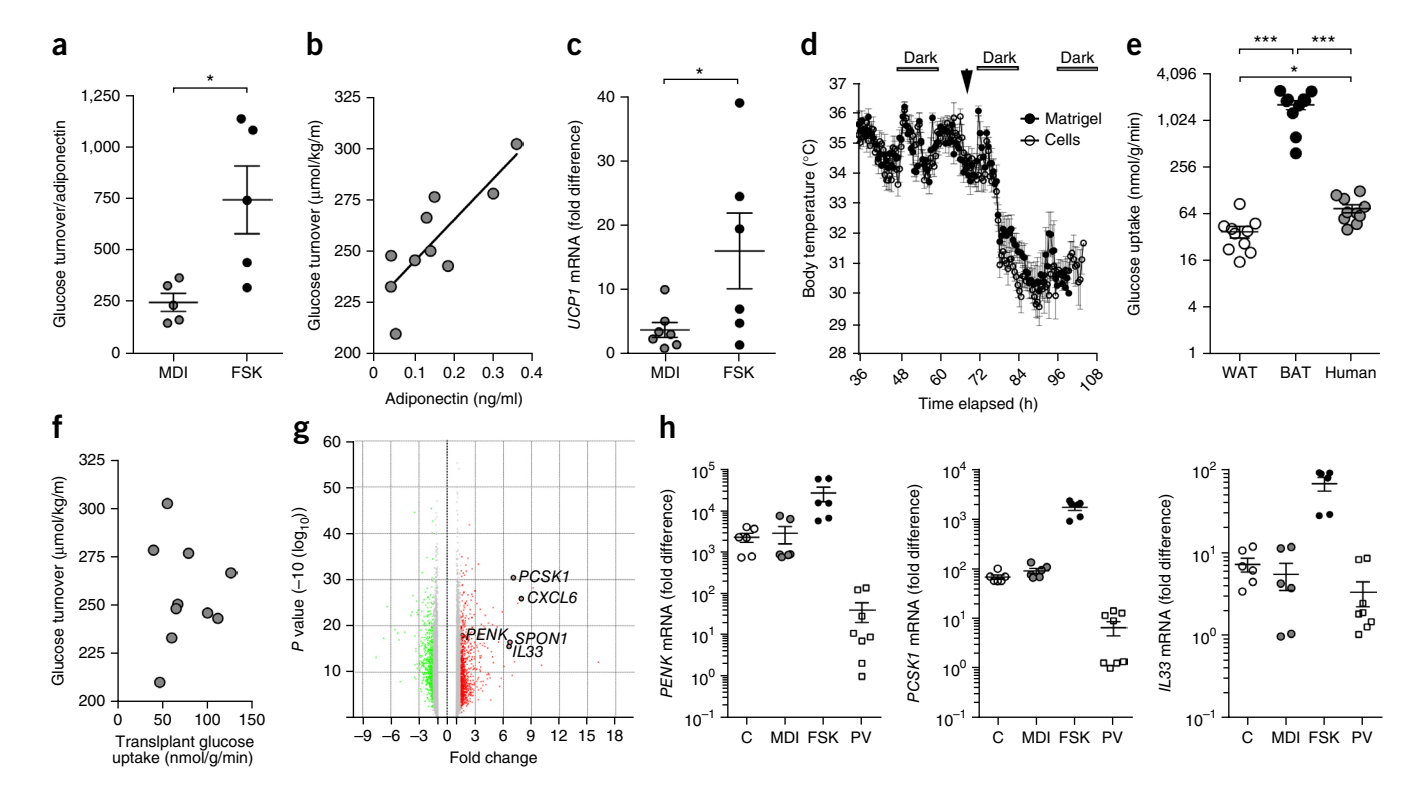


Figure 4 Mechanism for metabolic effects of human brite/beige adipocytes. (a) Glucose turnover (μ mol/kg/min) normalized to serum human adiponectin (ng/ml) in male mice implanted with nonstimulated (MDI, n=5) or with Fsk-stimulated (FSK, n=5) adipocytes, 7 weeks before hyperinsulinemic-euglycemic glucose clamps. Statistical analysis was performed using the Mann-Whitney test. *P < 0.05. (b) Relationship between serum human adiponectin levels and glucose turnover in implanted mice (n=10). Linear regression P value = 0.0027; $r^2 = 0.601$. (c) qPCR for human UCP1 in implanted cell structures from mice studied in **a**. Statistical analysis was done using unpaired two-tailed Student's t test. *P < 0.05. (d) Temperature recordings from subcutaneous iButtons in mice implanted with Matrigel or cells 7 weeks after implantation. Arrow represents time at which mice were placed at 5 °C. (e) Glucose uptake into epididymal fat (WAT), interscapular brown fat (BAT) and implanted cell structures from mice studied in **b**; n=10. Statistical analysis was performed using unpaired two-tailed Student's t test. *P < 0.05, ***P < 0.0001. (f) Relationship between glucose uptake into implanted cell structures and glucose turnover (n=10). (g) Volcano plot of differential gene expression in adipocytes without or with Fsk treatment for 7 d, indicating genes of interest. (h) qPCR of PCSK1, PENK and IL33 expression in nondifferentiated (C), differentiated (MDI) and Fsk-treated adipocytes (FSK), and perivascular adipose tissue (PV). Values represent fold difference over the lowest detectable value in the series for the respective probe set. Plotted are means \pm s.e.m. from two technical replicates of samples from three (cells) or four (PV) individuals.

which suggests that effects of the implanted cells on peripheral tissues contribute to enhanced whole-body glucose turnover. Indeed, improved metabolism attributable to the effects of brown adipose tissue on the liver has been reported²⁶.

To explore the possibility that the metabolic benefits of human brite/ beige adipocytes could be due to secreted factors, we conducted global gene-expression analysis of adipocytes before and after 7 d of Fsk stimulation (Fig. 4g). Unexpectedly, among the most significantly induced genes were the proprotein-convertase subtilisin/kexin type-1 (PCSK1), its substrate proenkephalin (PENK) and interleukin-33 (IL33), all of which were also detected in human pericarotid fat (Fig. 4h). Mutations and polymorphisms in PCSK1 are strongly associated with human obesity^{27,28}, although the underlying mechanisms are unclear. The cleavage of PENK by PCSK1 produces enkephalins, which are made in peripheral tissues in addition to in the brain²⁹. IL-33 has been shown in mouse models to decrease adiposity, mitigate atherosclerosis and be necessary for normal glucose homeostasis^{30,31}. Notably, enkephalins and IL-33 have been shown to induce adipose tissue browning³¹; thus, the production of these factors by implanted brite/beige cells could explain the sustained expression of UCP1 seen weeks after implantation (Fig. 3e). Although we were not able to detect IL-33 in the circulation of mice with transplanted cells, immunostaining revealed punctate structures containing IL-33 within activated

adipocytes (**Supplementary Fig. 4**). Further studies will be required to determine any possible autocrine effects of IL-33 on the induction or maintenance of the brite/beige adipocyte phenotype *in vivo*.

In summary, our data reveal that human adipocyte progenitor cells proliferate in response to pro-angiogenic stimuli in conjunction with adipose tissue angiogenesis. These cells display the cardinal feature of brite/beige adipocytes, which is a near absence of thermogenic genes under basal conditions, but strong induction in response to adrenergic stimulation. To our knowledge, these findings are the first to enable the growth and differentiation of human brite/beige cells *in vitro*, as well as to facilitate the assessment of these cells' effects on systemic glucose homeostasis in mice. These cells differ from human brown adipocyte cell lines established through the immortalization of human precursors^{32,33} or through the differentiation of human pluripotent stem cells³⁴ because of their highly inducible expression of a thermogenic phenotype, the development of uncoupled respiration and their capacity to affect metabolism upon transplantation *in vivo*.

Our finding of a functional relationship between angiogenesis and brite/beige adipocyte development converges with existing studies in which overexpression of the pro-angiogenic factor VEGF in mouse adipose tissue results in extensive browning^{35,36}. In addition, perivascular adipose tissue surrounding major blood vessels displays



thermogenic characteristics^{37,38}, and its loss results in cold intolerance, endothelial dysfunction and susceptibility to atherosclerosis in mice³⁷. The finding that human brite/beige adipocytes enhance glucose homeostasis provides a clear rationale for their potential therapeutic use. Moreover, the expression of neuroendocrine and secreted factors by activated cells suggests that the secreted products identified in these studies could also contribute to metabolic effects. Future studies to systematically assess the mechanisms by which human brite/beige cells develop and affect glucose homeostasis will be greatly facilitated by the ability to generate these cells from human adipose tissue by the methods described herein.

METHODS

Methods and any associated references are available in the online version of the paper.

Accession codes. Gene Expression Omnibus: Data files for Affymetrix HTA-2 arrays have been deposited with the accession number GSF73385

Note: Any Supplementary Information and Source Data files are available in the online version of the paper.

ACKNOWLEDGMENTS

This study was funded by US National Institutes of Health grants R01DK089101 (to S.C.), R24OD018259 (to M.A.B.), R01DK089185 (to M.P.C.), R01-DK080756, R01-DK079999, R24-DK090963 and U24-DK093000 (all to J.K.K.), and American Heart Association grant 12FTF11260010 (to T.F.). The authors acknowledge the use of the University of Massachusetts (UMASS) Flow Cytometry Core, the UMASS Genomics Core, the UMASS Mouse Phenotyping Center and the UMASS Morphology Core for conducting these studies.

AUTHOR CONTRIBUTIONS

S.Y.M., S.C., M.A.B. and M.P.C. designed the experiments; S.Y.M. and R.R.-R. obtained adipose tissue, generated cells and performed experiments on cells; J.K. and S.Y.M. performed experiments on mice; A.B., M.N., T.F. and M.P.C. obtained and analyzed perivascular adipose tissue samples; J.H.K., H.-L.N. and J.K.K. performed and analyzed metabolic phenotyping experiments. S.Y.M. and S.C. wrote the manuscript. All authors contributed to editing the manuscript. S.C. managed the project.

COMPETING FINANCIAL INTERESTS

The authors declare no competing financial interests.

Reprints and permissions information is available online at http://www.nature.com/reprints/index.html.

- 1. Collins, S. A heart-adipose tissue connection in the regulation of energy metabolism. *Nat. Rev. Endocrinol.* **10**, 157–163 (2014).
- Lee, Y.H., Petkova, A.P., Mottillo, E.P. & Granneman, J.G. *In vivo* identification of bipotential adipocyte progenitors recruited by β3-adrenoceptor activation and highfat feeding. *Cell Metab.* 15, 480–491 (2012).
- Shabalina, I.G. et al. UCP1 in brite/beige adipose tissue mitochondria is functionally thermogenic. Cell Reports 5, 1196–1203 (2013).
- Harms, M. & Seale, P. Brown and beige fat: development, function and therapeutic potential. Nat. Med. 19, 1252–1263 (2013).
- Nedergaard, J., Bengtsson, T. & Cannon, B. Unexpected evidence for active brown adipose tissue in adult humans. Am. J. Physiol. Endocrinol. Metab. 293, E444–E452 (2007).
- Cypess, A.M. et al. Identification and importance of brown adipose tissue in adult humans. N. Engl. J. Med. 360, 1509–1517 (2009).
- van Marken Lichtenbelt, W.D. et al. Cold-activated brown adipose tissue in healthy men. N. Engl. J. Med. 360, 1500–1508 (2009).
- Lidell, M.E., Betz, M.J. & Enerbäck, S. Two types of brown adipose tissue in humans. Adipocyte 3, 63–66 (2014).

- Crandall, D.L., Hausman, G.J. & Kral, J.G. A review of the microcirculation of adipose tissue: anatomic, metabolic, and angiogenic perspectives. *Microcirculation* 4, 211–232 (1997).
- Han, J. et al. The spatiotemporal development of adipose tissue. Development 138, 5027–5037 (2011).
- 11. Bouloumié, A., Lolmède, K., Sengenès, C., Galitzky, J. & Lafontan, M. Angiogenesis in adipose tissue. *Ann. Endocrinol. (Paris)* **63**, 91–95 (2002).
- Tang, W. et al. White fat progenitor cells reside in the adipose vasculature. Science 322, 583–586 (2008).
- Gupta, R.K. et al. Zfp423 expression identifies committed preadipocytes and localizes to adipose endothelial and perivascular cells. Cell Metab. 15, 230–239 (2012).
- 14. Gealekman, O. et al. Depot-specific differences and insufficient subcutaneous adipose tissue angiogenesis in human obesity. Circulation 123, 186–194 (2011).
- Tran, K.V. et al. The vascular endothelium of the adipose tissue gives rise to both white and brown fat cells. Cell Metab. 15, 222–229 (2012).
- van de Vyver, M., Andrag, E., Cockburn, I.L. & Ferris, W.F. Thiazolidinedione-induced lipid droplet formation during osteogenic differentiation. *J. Endocrinol.* 223, 119–132 (2014).
- 17. Wu, J. et al. Beige adipocytes are a distinct type of thermogenic fat cell in mouse and human. Cell 150, 366–376 (2012).
- Cypess, A.M. et al. Activation of human brown adipose tissue by a β3-adrenergic receptor agonist. Cell Metab. 21, 33–38 (2015).
- 19. Cousin, B. et al. Occurrence of brown adipocytes in rat white adipose tissue: molecular and morphological characterization. J. Cell Sci. 103, 931–942 (1992).
- Orlicky, D.J., Monks, J., Stefanski, A.L. & McManaman, J.L. Dynamics and molecular determinants of cytoplasmic lipid droplet clustering and dispersion. *PLoS One* 8, e66837 (2013).
- Marcinkiewicz, A., Gauthier, D., Garcia, A. & Brasaemle, D.L. The phosphorylation of serine 492 of perilipin a directs lipid droplet fragmentation and dispersion. *J. Biol. Chem.* 281, 11901–11909 (2006).
- Zhang, Y., Matheny, M., Zolotukhin, S., Tumer, N. & Scarpace, P.J. Regulation of adiponectin and leptin gene expression in white and brown adipose tissues: influence of beta3-adrenergic agonists, retinoic acid, leptin and fasting. *Biochim. Biophys. Acta* 1584, 115–122 (2002).
- Behan, J.W. et al. Activation of adipose tissue macrophages in obese mice does not require lymphocytes. Obesity (Silver Spring) 21, 1380–1388 (2013).
- Xiao, C., Goldgof, M., Gavrilova, O. & Reitman, M.L. Anti-obesity and metabolic efficacy of the β3-adrenergic agonist, CL316243, in mice at thermoneutrality compared to 22°C. Obesity (Silver Spring) 23, 1450–1459 (2015).
- Hocking, S.L. et al. Subcutaneous fat transplantation alleviates diet-induced glucose intolerance and inflammation in mice. Diabetologia 58, 1587–1600 (2015).
- Wang, G.X. et al. The brown fat-enriched secreted factor Nrg4 preserves metabolic homeostasis through attenuation of hepatic lipogenesis. Nat. Med. 20, 1436–1443 (2014).
- Jackson, R.S. et al. Obesity and impaired prohormone processing associated with mutations in the human prohormone convertase 1 gene. Nat. Genet. 16, 303–306 (1997)
- Benzinou, M. et al. Common nonsynonymous variants in PCSK1 confer risk of obesity. Nat. Genet. 40, 943–945 (2008).
- Denning, G.M. et al. Proenkephalin expression and enkephalin release are widely observed in non-neuronal tissues. Peptides 29, 83–92 (2008).
- 30. Miller, A.M. *et al.* Interleukin-33 induces protective effects in adipose tissue inflammation during obesity in mice. *Circ. Res.* **107**. 650–658 (2010).
- Brestoff, J.R. *et al.* Group 2 innate lymphoid cells promote beiging of white adipose tissue and limit obesity. *Nature* 519, 242–246 (2015).
- Shinoda, K. et al. Genetic and functional characterization of clonally derived adult human brown adipocytes. Nat. Med. 21, 389–394 (2015).
- Xue, R. et al. Clonal analyses and gene profiling identify genetic biomarkers of the thermogenic potential of human brown and white preadipocytes. Nat. Med. 21,
- 760–768 (2015).34. Nishio, M. et al. Production of functional classical brown adipocytes from human pluripotent stem cells using specific hemopoietin cocktail without gene transfer.
- Cell Metab. 16, 394–406 (2012).
 35. Elias, I. et al. Adipose tissue overexpression of vascular endothelial growth factor protects against diet-induced obesity and insulin resistance. Diabetes 61, 1801–1813 (2012).
- Sun, K. et al. Dichotomous effects of VEGF-A on adipose tissue dysfunction. Proc. Natl. Acad. Sci. USA 109, 5874–5879 (2012).
- Chang, L. et al. Loss of perivascular adipose tissue on peroxisome proliferator-activated receptor-γ deletion in smooth muscle cells impairs intravascular thermoregulation and enhances atherosclerosis. *Circulation* 126, 1067–1078 (2012).
- Fitzgibbons, T.P. et al. Similarity of mouse perivascular and brown adipose tissues and their resistance to diet-induced inflammation. Am. J. Physiol. Heart Circ. Physiol. 301, H1425–H1437 (2011).



ONLINE METHODS

General methodology. No samples, mice or data points were excluded from the reported analyses. Samples were not randomized to experimental groups except where indicated. Analyses were not performed in a blinded fashion except where noted below.

Materials. Matrigel from BD Biosciences (356231); EGM-2 MV from Lonza; Anti-human UCP1 antibody from Abcam (ab10983); anti-heat shock protein 70 from ThermoFisher Scientific (MA3-028); anti-human IL33 from ThermoFisher Scientific (PA5-20397); Adiponectin human-specific ELISA kits from Invitrogen (KHP0041); Forskolin and Isoproterenol hydrochloride from Sigma (F3917 and I6504, respectively). iButtons were purchased from Embedded Data Systems, DS1922L-F5#).

Adipose tissue. Subcutaneous adipose tissue was obtained from panniculectomies, and pericarotid adipose tissue was obtained from elective vascular surgeries with no selection of individual donors *a priori*. All specimens were collected after obtaining informed consent in accordance with procedures approved by the University of Massachusetts Institutional Review Board. The characteristics of patients from whom tissues were used for indicated experiments are described in **Supplementary Table 1**.

Explants. Detailed methods for the harvesting of adipose tissue and for the culture of adipose tissue explants in Matrigel are published³⁹. In brief, explants from human subcutaneous adipose tissue were cultured in EBM-2 media supplemented with endothelial growth factors (EGM-2 MV) (Lonza). In indicated experiments, Dulbecco's Modified Eagle's Medium (Gibco) supplemented with 10% FBS ((DMEM-FBS) was used, without or with supplementation with hFGF-B, hEGF, R3-IGF1 and VEGF at the concentrations used in EGM2-MV, as indicated. To quantify growth by image analysis, we subtracted the area occupied by the sprouts on day 3 from that at day 10. We observed cell loss over time in some of the explants cultured in the absence of angiogenic growth factors, which resulted in negative values. To induce adipogenesis, we used a minimal adipogenic cocktail of DMEM + 10% FBS, 0.5 mM 3-isobutyl-1methylxanthine, 1 μ M dexamethasone and 1 μ g/ml insulin (MDI) for 72 h. The medium was then replaced with DMEM + 10% FBS. Subsequently, 50% of the medium was replaced with fresh medium every other day. Adipocyte markers were measured by qPCR in RNA extracted from three explants per condition. Results shown in Figure 1 were reproduced in explants from all panniculectomy samples studied (Supplementary Table 1), although the magnitude of the induction of individual markers varied.

Cells. Detailed methods for harvesting adipose tissue, culturing adipose tissue explants in Matrigel and harvesting single cells from explant growth are published³⁹. In brief, explants from human subcutaneous adipose tissue were cultured in EBM-2 medium supplemented with endothelial growth factors (EGM-2 MV) (Lonza) for 14 d. Single-cell suspensions from capillary growth (capillary network cells) were obtained using dispase³⁹, and these were plated on standard tissue culture plates. Growth and passaging of these cells was done using EGM-2 MV. Where indicated, adipogenic differentiation was induced by the replacement of EGM-2 MV with DMEM + 10% FBS, 0.5 mM 3-isobutyl-1-methylxanthine, 1 µM dexamethasone and $1 \mu g/ml$ insulin (MDI). Seventy-two hours later, the differentiation medium was replaced by DMEM-FBS, which was replaced every 48 h until analysis. Adipocyte markers were measured by means of qPCR in RNA extracted from one well of a confluent six-well multiwell dish of cells. To obtain clonal populations, single-cell suspensions were obtained from capillary network cell cultures using trypsin, and then stained with 7-amino-actinomycin D (7-AAD) for live/dead cell identification, and sorted into individual wells of 384-well multiwell dishes by using a BSL3 BD FACSAria Cell Sorter (BD Biosciences). Clones were grown and expanded using EGM-2 MV. Viable clones were passaged onto 96-well multiwell dishes, which were differentiated as described above and used for the experiments described. Cells were not routinely tested for mycoplasma contamination. Adiponectin concentration in the culture medium was measured using a humanspecific adiponectin ELISA from Invitrogen (KHP0041). For analysis of thermogenic gene expression, isoproterenol and Fsk were used at final concentrations of 10 and 50 $\mu M,$ unless otherwise indicated in the figures.

In experiments to investigate the effects of brite/beige adipocytes *in vivo*, cells from capillary networks were grown to confluence into 150-mm dishes and differentiated using MDI for 10 d, and browning was induced for 7 d with Fsk. Cells were then were recovered from culture dishes by means of trypsin-collagenase digestion, suspended in Matrigel and injected ($\sim 10^7$ cells per mouse) into the dorsal region of male NSG mice⁴⁰.

qPCR. Adipocyte markers were measured in RNA extracted from three explants per condition, or from one well of a confluent six-well multiwell dish of cells. Probe sets used are shown in **Supplementary Table 2**.

Immunofluorescence. Cells were fixed in 4% formaldehyde and then stained, mounted and imaged with a Zeiss Axiovert 100 inverted microscope and an AxioCam HRm camera. Image processing and quantification was performed using ImageJ (FIJI) software, on a file that contained all raw images to be analyzed and thereby applied all corrections equally for all comparison groups. After background subtraction, the gray scale image is converted into a binary image, and the sum of white pixels in each individual image is recorded.

Oxygen consumption. Oxygen consumption and mitochondrial parameters in intact cells were obtained using the XF24 Extracellular Flux Analyzer, which was equipped with a FluxPak mini kit (#100867-100) from Seahorse Biosciences. In this system, oxygen consumption rates are calculated from four independent measurements obtained at 5-min intervals at baseline and after the addition of specific drugs. For each experiment, the means from three replicate wells were recorded. For the assessment of mitochondrial parameters, the values for the four independent measurements recorded for each condition were averaged, and parameters were calculated as follows: ATPlinked respiration = basal OCR - oligomycin OCR; proton leak = oligomycin OCR - (rotenone + antimycin OCR); maximal capacity = FCCP OCR; reserve capacity = FCCP OCR - basal OCR; nonmitochondrial respiration = rotenone + antimycin OCR. Values presented are the means and s.e.m. of four independent experiments. For assessment of GDP sensitivity, cells were detached using trypsin-collagenase and suspended in respiration buffer⁴¹, permeabilized with 20 $\mu g/ml$ digitonin in respiration buffer for 5 min and washed again. Oxygen consumption was measured at 1 s intervals using a Clark-type Oxygraph Plus recorder (Hansatech Instruments). Oxygen consumption rates were expressed as the slopes of the linear regression fits for each trace, derived from a minimum of 300 points, after each addition. GDP was used at a final concentration of 1 mM.

Mice. All animal use was in accordance with the guidelines of the Animal Care and Use Committee of the University of Massachusetts Medical School. For all experiments reported, male NOD.Cg-PrkdcscidIl2rgtm1Wjl/SzJ (NOD-scid $IL2r\gamma^{\text{null}}$, NSG) mice⁴⁰ were used, at 12–14 weeks of age. Mice were obtained from the Jackson Laboratory. Mice were injected subcutaneously with Matrigel or with cells suspended in Matrigel. After the times indicated, animals were sacrificed and tissues were removed for further study. Where indicated, mice were fed 60% HFD (Research Diets, Inc. D12492). Glucose-tolerance curves were obtained with 2 g/kg glucose after 8 h or 16 h fasting, as indicated. The sample sizes chosen for glucose-tolerance tests, temperature recordings and hyperinsulinemic-euglucemic clamp studies were based on preliminary data in control mice to determine variance for each parameter. Male animals of similar age, bred under the same conditions, were randomly assigned to Matrigel or cells, and, of those assigned to cells, to nonstimulated or Fsk-stimulated cells, and the investigator who conducted the glucose-tolerance tests, hyperinsulinemic-euglycemic clamps and serum adiponectin measurements was blinded to the group (Matrigel or cells, and normal diet or HFD) allocation.

Affymetrix arrays. Total RNA was isolated using TRIzol. Affymetrix protocols were followed for the preparation of cRNA, which was hybridized to HTA-2.0 arrays. Raw expression data collected from an Affymetrix HP GeneArrayScanner was normalized across all data sets using the RMA algorithm as implemented by the Affymetrix Expression Console.



NATURE MEDICINE doi:10.1038/nm.4031

Expression analysis was performed using the Affymetrix Transcriptome Analysis Console v.3.0. The data discussed in this publication have been deposited in the National Center for Biotechnology Information (NCBI) Gene Expression Omnibus and are accessible with GEO Series accession number GSE73385.

Hyperinsulinemic-euglycemic clamp. Survival surgery was performed at 5 or 6 d before clamp experiments to establish an indwelling catheter in the jugular vein. On the day of the clamp experiment, mice were fasted overnight (~15 h), and a 2-h hyperinsulinemic-euglycemic clamp was conducted in conscious mice with a primed and continuous infusion of human insulin (150 mU/kg body-weight priming followed by 2.5 mU/kg/min; Humulin, Eli Lilly & Co., Indianapolis, Indiana, USA). To maintain euglycemia, 20% glucose was infused at variable rates during clamps. Whole-body glucose turnover was assessed with a continuous infusion of [3- 3 H]-glucose (PerkinElmer, Waltham, Massachusetts, USA), and 2-7deoxy-D-[1- 1 4C]-glucose (2-[1 4C]-DG) was administered as a bolus (10 μ Ci) at 75 min after the start of clamps to measure insulin-stimulated glucose uptake in individual organs.

Statistical analyses. qPCR results are presented as means of technical replicates with error ranges indicated. Experiments shown are representative, and

they were repeated a minimum of five times with cells derived from different individuals undergoing panniculectomy surgery, with no *a priori* selection. The number of animals used for glucose-tolerance tests, for temperature recordings and for hyperisnulinemic-euglucemic clamp studies was chosen on the basis of preliminary data in normal control mice to determine variance for each parameter. Software employed was GraphPad Prism v.6. To compare groups with normally distributed values, the two-tailed unpaired Student t test was used. When normality could not be determined, the Mann-Whitney test was used. Data are presented as mean values \pm s.e.m., or range between technical replicates when experiments were representative, as indicated in each figure legend. P values are indicated in each case. All representative experiments have been repeated a minimum of five times with tissue from different individuals, with similar results.

- 39. Rojas-Rodriguez, R. *et al.* Adipose tissue angiogenesis assay. *Methods Enzymol.* **537**, 75–91 (2014).
- Brehm, M.A. et al. Engraftment of human HSCs in nonirradiated newborn NOD-scid IL2ry^{null} mice is enhanced by transgenic expression of membrane-bound human SCF. Blood 119, 2778–2788 (2012).
- 41. Shabalina, I.G., Kramarova, T.V., Nedergaard, J. & Cannon, B. Carboxyatractyloside effects on brown-fat mitochondria imply that the adenine nucleotide translocator isoforms ANT1 and ANT2 may be responsible for basal and fatty-acid-induced uncoupling respectively. *Biochem. J.* 399, 405–414 (2006).



doi:10.1038/nm.4031